

# Computational and Experimental Study of the Flow in the Scaled Diffuser Models of the Air Force Subsonic Aerodynamic Research Laboratory Wind Tunnel

**Devon Miller**

Aerospace Engineering and Mechanics Dept.  
The University of Alabama  
Tuscaloosa, Alabama, USA

**Muhammad A R Sharif**

Aerospace Engineering and Mechanics Dept.  
The University of Alabama  
Tuscaloosa, Alabama, USA

**Semih Olcmen**

Aerospace Engineering and Mechanics Dept.  
The University of Alabama  
Tuscaloosa, Alabama, USA

**Ryan H. Weiner**

Aerospace Engineering and Mechanics Dept.  
The University of Alabama  
Tuscaloosa, Alabama, USA

**Christopher D. King**

GE Aviation, Military Control Systems  
Lynn, Massachusetts, USA

**Abstract**—Computational and experimental analysis of the diffuser flow, conducted on 1:60 scale models of the diffuser section of the Air Force Subsonic Aerodynamic Research Laboratory (SARL) wind tunnel, are reported. ANSYS Fluent CFD code is used to compute the turbulent flow fields in small scale models of four diffuser geometries, identified in a previous numerical research with full scale models of these diffusers. One of the models replicates the existing SARL wind tunnel diffuser. Experiments are conducted to measure the velocity distribution in the diffuser wake for the 3D printed small scale models of the same four diffuser geometries. Comparison of the predicted and experimental velocity distributions are made to assess the validity of the numerical model and the associated numerical methods. The performance of the models is evaluated based on the total pressure recovery between the inlet and the diffuser exit sections. Results indicate that the predicted and the experimental wake velocity distribution obtained in the current study match reasonably well. The predicted total pressure drop for each model indicate that the computations for the full scale models of the previous study and that for the small scale models of the present study identify the same diffuser geometry as the most efficient diffuser configuration (producing lowest total pressure drop) to improve the efficiency of the existing SARL tunnel.

**Keywords**—wind tunnel, diffuser flow, numerical simulation, efficiency increase, turbulent flow,  $k-\epsilon$  model

## I. INTRODUCTION

Diffusers are used in many industrial applications ranging from jet engines to air-conditioning systems, and are used to reduce the velocity along the axis of the diffuser while recovering the static pressure [1, 2]. Diffusers are used downstream of wind tunnel test sections to reduce the power consumption [3, 4], downstream of compressors, fans and turbines to increase the efficiency of such devices [5-7], in the design of efficient micro-pumps, [8], and in inlet designs [9]. Diffusers are, in general, two-dimensional rectangular [10], conical [11], annular [12], and radical-(an S duct with rectangular entrance and circular exit) [9] in shape, and are designed and used based on the internal flow application at hand. The research on the diffusers continues since diffusers modify the flow field in devices they are used in as an integral part of that device.

The current research is the continuation of a previous work [13], which aimed at investigating alternative diffuser geometries to determine a unique diffuser that would increase the efficiency of the large wind tunnel located at the Wright-Patterson Air Force Base in Dayton, Ohio. The Subsonic Aerodynamic Research Laboratory (SARL) wind tunnel [14], which was designed to operate up to Mach = 0.6 (but limited to Mach 0.5), is driven by a 20,000 HP motor. The details of the SARL tunnel are available in the aforementioned paper by King et al. [13]. Previous analysis of cumulative losses throughout the tunnel indicated that approximately 30% of all losses in the tunnel occurred at the tunnel exit [15]. In that work, the geometry of the entire tunnel was considered and the losses were expressed using a section total pressure loss coefficient given as:

$$K_0 = \frac{\Delta p_0}{q_{ts}} = K \frac{q_{local}}{q_{ts}} = K \left( \frac{V_{local}}{V_{ts}} \right)^2 \quad (1)$$

where  $\Delta p_o$  is the change in total pressure across a given location,  $q_{ts}$  is the dynamic pressure at the test section,  $q_{local}$  is the dynamic pressure at a specified location,  $K$  is the local total pressure loss coefficient,  $V_{ts}$  is the velocity magnitude at the test section, and  $V_{local}$  is the velocity magnitude at a specified location, respectively. The results of the work by Britcher [15], showed that the existing SARL tunnel system with the existing diffuser design, has a cumulative loss coefficient of about 0.245. The study concluded that the circuit losses were "dominated" by the diffuser and exit sections of the tunnel. If the exit loss coefficient could be reduced, a significant reduction in losses could be observed for the entire tunnel, up to approximately 16% reduction based on analytical study by Britcher [15].

The previous research of King et al. [13] was thus focused on minimizing the losses by modifying the diffuser of the wind tunnel. In order to achieve this goal, several diffuser geometries were identified and evaluated for effectiveness in loss reduction. Computational methods were used due to the very large size of the tunnel which prohibits experimental evaluation of those geometries. Preliminary computations were made using SolidWorks/FloWorks CAD program [16]. Numerical models of over thirty widely varying diffuser geometries were developed based on previous knowledge on diffuser geometries [3,4,7,17-20], which were evaluated for effectiveness in reducing losses for the SARL tunnel. Literature survey showed that previous systematic research undertaken on conical diffusers was mainly focused on studying empty conical diffusers [11,17,19-21]. These studies indicated that, (i) the ratio of the exit to entrance areas and the length of the diffuser are the parameters directly affecting the pressure recovery performance of the conical diffusers [19] (ii) the pressure recovery becomes independent of the Reynolds number over  $Re = 75000$  [22,23], and (iii) the diffusers with apex angle  $\sim 7^\circ$  has the best performance [22]. Research on the annular conical diffusers was focused on investigation of different configurations for specific applications [12,24-28].

Out of the 30 different diffuser geometries analyzed by the FloWorks code, four specific geometries were selected for more detailed and accurate analysis by the ANSYS FLUENT code [29]. These included the existing SARL diffuser (baseline model) with an  $8^\circ$  half-apex angle, henceforth termed as "8BT," and a modified version of it with a  $3.5^\circ$  half-apex angle, henceforth termed as "35BT." The 35BT was also modified simply by adding a constant area flat diffuser at the end, henceforth termed as "35F" which was further modified with an additional annular conical diffuser after the flat section, henceforth termed as "35FC". The 35FC consisted of three concentric truncated cones with included angles of  $60^\circ$ ,  $34.7^\circ$ ,  $17.2^\circ$ , and the entrance area to the inner cone was equal to the entrance areas between the successive cones. For the 35FC model, the flat and the conical sections had the same length. The 35F and the 35FC configurations were selected because they produced greatest reduction in pressure losses and about 6% improvement in the entire tunnel efficiency when

analyzed with the FloWorks code. These four diffuser configurations are shown in Fig. 1. Full scale diffuser dimensions of the existing SARL tunnel was used in the computational models [13]. The Reynolds number for these computations is based on the average inlet velocity and the duct diameter at the inlet section for air at  $15^\circ\text{C}$ . The Reynolds number for the full scale numerical models was taken as  $1.647 \times 10^7$ .

The results indicated that a  $3.5^\circ$  half-apex angle conical diffuser followed with tubular and annular conical section with dividers (35FC) results in the least total pressure loss. The calculated percent head loss reductions for this diffuser geometry ranged from 14.9% to 20.9% over the existing SARL diffuser geometry. For the entire SARL tunnel, this corresponds to a substantial 5.2% to 7.3% efficiency improvement.

The objective of this present study is to obtain experimental data and conduct numerical analysis/simulation on the AF-SARL tunnel diffuser flow. As mentioned earlier, due to very large size of the prototype SARL tunnel and diffuser and its unavailability because of heavy uses by the Air Force, full scale experimental investigation is not practicable. For this reason, the full scale model computational results of King et al. [13] could not be validated. Hence, it was decided to build small scale models of a few selected diffuser designs and conduct experimental measurements on the associated flow processes. These small scale models correspond to the same 4 large scales models, viz., 8BT, 35BT, 35F, and 35FC, which were numerically investigated by King et al. . These models with a 1:60 scale were manufactured in the 3D printer of WPAFB-AFRL facilities. The results of these measurements and subsequent numerical simulation are presented here. Numerical computations of the flow through these four small scale diffuser models are conducted using the ANSYS FLUENT code. The results are compared with the experimental measurements for the validation of the simulation process. The diffuser design producing lowest pressure drop is identified.

## II. EXPERIMENTAL SETUP

Experimental setup included a PVC pipe equipped with an ejector pump. The pipe was long enough to result in a fully developed velocity profile at the exit. The small scale diffuser models were attached to the exit of the pipe. Total pressure measurements were made on a cross-sectional plane located 3.175 mm (1/8 inch) downstream of the drive shaft extension of the diffuser. Total pressure measurements were used to calculate the flow velocity using the Bernoulli's equation and assuming that the static pressure is the atmospheric pressure since the measurement station is in the open domain outside of the diffuser casing.

### A. Experimental Instrumentation

Experimental setup is shown in Fig. 2. Motive air required for the experiments was supplied from a  $28.3 \text{ m}^3$  ( $1000 \text{ ft}^3$ ) tank that can be pressurized up to 1,379 kPa (200 psi) absolute. The pressurized air was lead to a Wilkerson pressure regulator that was used to set the regulator output pressure. Regulator output was

directed to the VACCON CDF 750H-EPT107 ejector pump using additional Tygon tubing. Ejector pump inserted into the PVC pipe was used to generate 60 m/s uniform inlet velocity to the pipe. The ejector pump generates a high output flow using a smaller volume of compressed air utilizing the Coanda effect and the flow rate passing through the pump can be manipulated by adjusting the motive air flow rate.

The flow velocity in the pipe was adjusted using pressure values read from a Pitot tube inserted into the

flow and a static port located 25.4 mm (1 inch) upstream of the pipe exit. Pressure difference between the Pitot tube and the static port readings was used to set the pipe center velocity. At this axial location the center velocity was set to 72.5 m/s by adjusting the ejector-pump supply pressure using the pressure regulator to ensure a constant velocity. During the experiments the

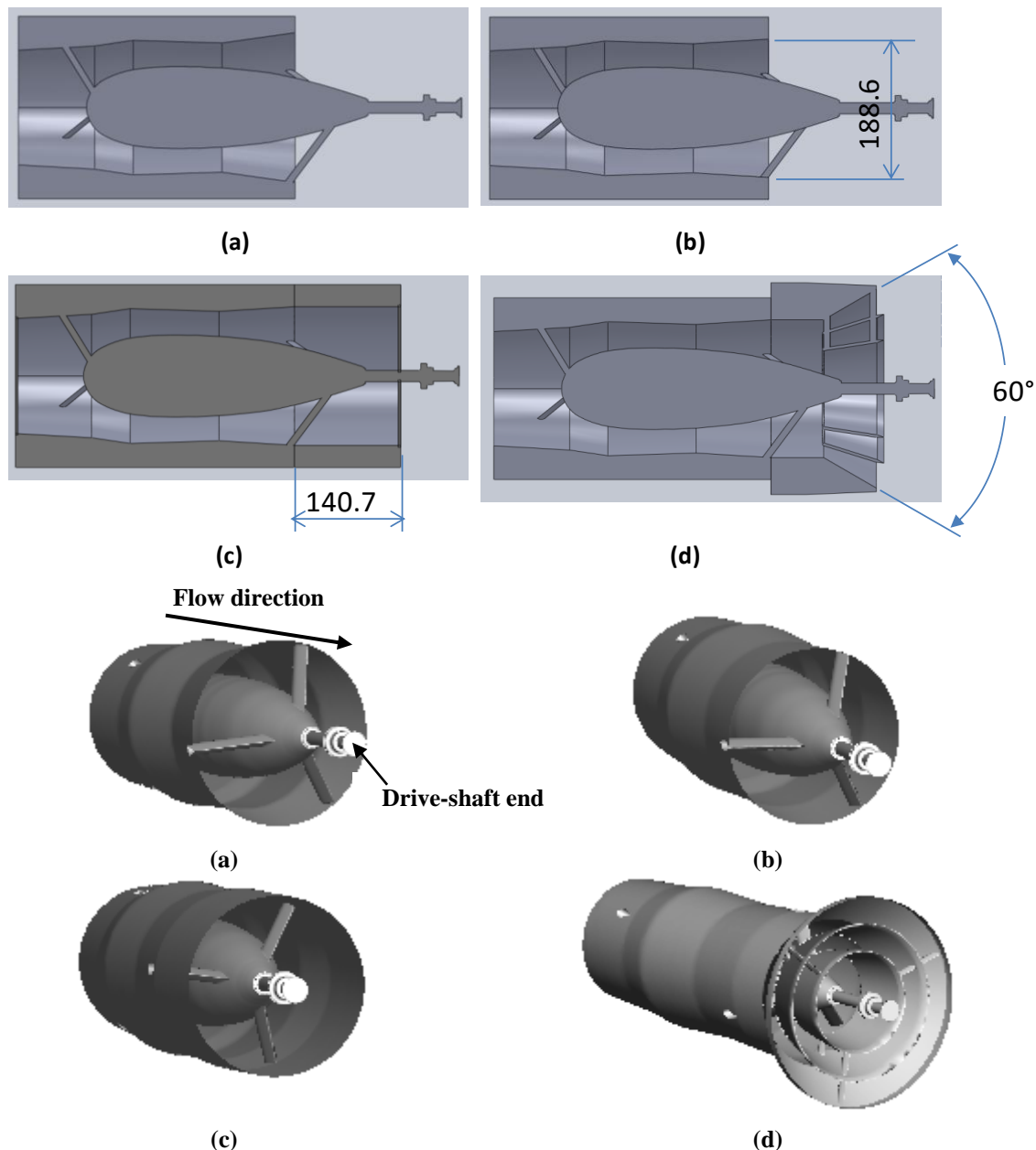


Fig. 1. Top: Sectional views of the 4 diffuser configurations; a) 8BT, b) 35BT, c) 35F, d) 35FC (reproduced from King et al. (2013)). Bottom: corresponding isometric views looking from the diffuser exit end.

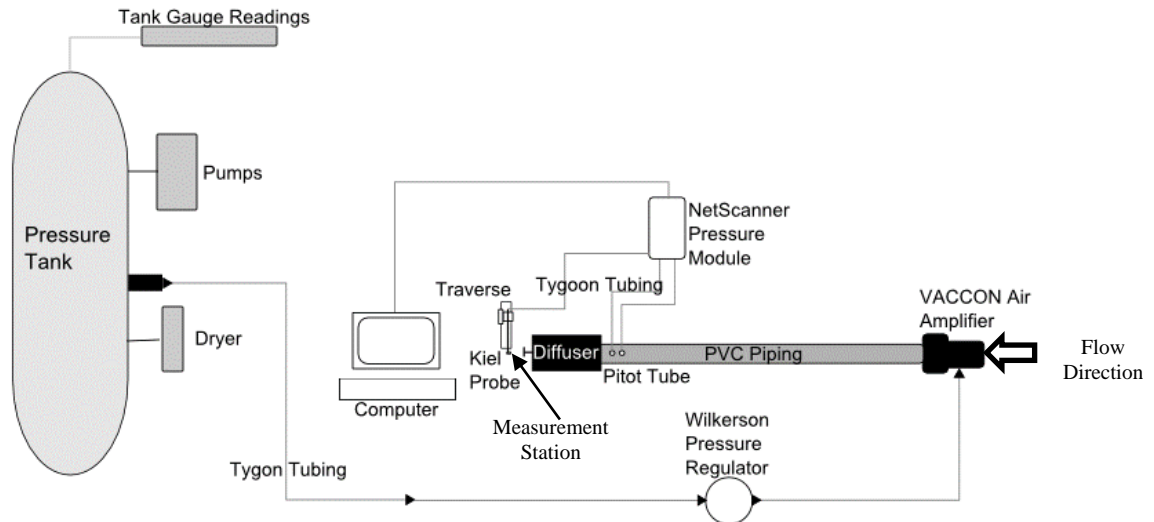


Fig. 2. Experimental setup.

Pitot tube was removed to not to disturb the flow. Pressures were read using NetScanner model 9016. The data was reduced using NetScanner Unified Startup Software (NUSS).

The diffuser attachments were connected to the exit of the PVC pipe and secured in place using hose clamps. The total pressure was measured with a Kiel probe (United Sensor, KBC-12-F-10-C) connected to a manual traversing together with the NetScanner pressure transducer system. Kiel probe design includes a Pitot tube within a shroud resulting in pressure readings less sensitive to changes in the flow angularity up to  $20^\circ$ .

The data was obtained on a  $xy$  plane (plane parallel to the diffuser exit plane) at 3.175 mm (1/8 in) downstream of the drive shaft end of the diffuser (see Fig. 1 bottom part and Fig. 2 for the measurement station). Measurements at this plane were made on a 3.175 mm  $\times$  3.175 mm square grid along the  $x$  and  $y$  axes covering a range of  $(-0.5D \leq x \leq 0.5D$  and  $-0.5D \leq y \leq 0.5D)$  where  $D$  is the diffuser casing diameter at the exit. The  $x$  axis was parallel to the room floor, the  $y$  axis was perpendicular to the floor, and the  $z$  axis was in the flow direction along the axis of the diffuser.

The length of the pipe was chosen to achieve a turbulent fully developed flow at the exit of the pipe. This length was taken greater than the pipe entry length,  $l_e$ , determined using the expression  $l_e/D = 4.4Re^{1/6}$  where  $Re = \rho VD/\mu$  is the Reynolds number, defined in terms of the average velocity in the pipe ( $V$ ), the pipe diameter ( $D$ ), fluid density ( $\rho$ ), and the dynamic viscosity ( $\mu$ ). The pipe used was a schedule 40 PVC pipe with an inner diameter of  $D = 0.04$  m to match the diameter of the diffuser at the entrance section. The pipe inlet uniform velocity was set to  $V = 60$  m/s. The Reynolds number used for the small scale models was  $Re = 153,617$  (with  $\rho = 1.184$  kg/m<sup>3</sup> and  $\mu = 1.85 \times 10^{-5}$  N s/m<sup>2</sup>) based on which the corresponding

entry length,  $l_e = 1.288$  m. A slightly longer pipe length of 1.34 m was used in the experiment.

The fully developed profile for the axial velocity,  $v$  can be expressed as

$$\frac{v}{V_c} = \left(1 - \frac{r}{R}\right)^{1/n} \quad (2)$$

where  $V_c$  is the centerline velocity,  $r$  is the radial distance,  $R$  is the pipe inner radius, and  $n$  is an exponent whose value depends on the Reynolds number. The value of  $n$  for  $Re = 153,617$  is found to be 7.5 [30]. The equation for the average velocity in the pipe,  $\bar{v}$ , for this profile can be calculated using

$$\frac{\bar{v}}{V_c} = \frac{2n^2}{(n+1)(2n+1)} \quad (3)$$

from which the centerline velocity  $V_c$  is obtained as 72.5 m/s for the given average velocity of 60 m/s and  $n = 7.5$ .

### B. The Experimental Uncertainty

Uncertainty analysis was conducted using the Kline and McClintock [31] method. The reported velocity magnitude values were calculated using the Bernoulli's equation as

$$V = \sqrt{\frac{2(P_o - P)}{\rho}} \quad (4)$$

where  $P_o$  is the total pressure and  $P$  is the atmospheric pressure. The air density,  $\rho$ , was calculated using the ideal gas relation. The full scale range of the NetScanner transducers used to measure the pressures was 10 inches of water (2,500 Pa) and the uncertainty of the transducers was 0.05% ( $\pm 12.5$  Pa). Temperature uncertainty was  $\pm 0.1$  K. The velocity measurement uncertainty was determined using Eq. (5) as

$$\Delta V = \sqrt{\left(\frac{1}{\rho V} * \Delta P_o\right)^2 + \left(-\frac{1}{\rho V} * \Delta P\right)^2 + \left(-\frac{V}{2\rho} * \sqrt{\left(-\frac{1}{\rho U} \Delta P\right)^2 + \left(-\frac{\rho}{T} \Delta T\right)^2}\right)^2}$$

(5)

The values for the average velocity uncertainty for each of the four cases studied ranged from 0.84% - 2.03%.

### III NUMERICAL PROCEDURE AND PROBLEM SETUP

The Reynolds-Averaged Navier-Stokes (RANS) equations were solved using the ANSYS FLUENT commercial code with the standard  $k-\epsilon$  turbulence model with enhanced wall treatment (as implemented in the FLUENT code). Since the primary goal of the computations here is to compare the performance of the four chosen diffuser models in terms of the pressure loss without being too concerned about the accuracy of the results; more sophisticated turbulence models such as RNG  $k-\epsilon$  or SST  $k-\omega$  model, etc., (needing much more computational time for the complicated domain and mesh considered) are not used. The governing equations and turbulence model constants are available in FLUENT user manual and are not repeated here. The flow domain is divided into many small finite volumes with a tetrahedral unstructured mesh. A collocated arrangement for the placement of the flow variables is used in the mesh system. The conservation equations are integrated over each of the finite volume to yield sets of linear algebraic equations. These sets of linear algebraic equations are then solved sequentially using an iterative method. The SIMPLE algorithm is used for the pressure-velocity coupling. The convective fluxes have been calculated using the second order upwind scheme while the diffusive fluxes have been calculated using the central difference scheme. The convergence is assumed when the value of the scaled residual of continuity and momentum equations is less than  $10^{-6}$ . Convergence has also been monitored by plotting the drag on the nacelle surface until the variation of the drag leveled off with iteration.

In the prototype configuration, there are fan blades attached to the rotating nacelle during tunnel operations. In the computations, the effects of the blade rotation on the flow field were excluded since it would have required very large computational resources. The blades were also excluded from the geometry to study the effects of only the diffuser geometry on the efficiency calculations.

#### A. Geometry and Mesh Design

The flow configuration geometry was created using the SolidWorks code [16] which was imported into ANSYS FLUENT [29] for mesh generation. The computational mesh was generated using the meshing code integrated in the ANSYS package. The solid bodies, such as the outer diffuser, fan duct wall, engine nacelle, and support spars had a "face sizing" mesh control applied to these surfaces, with a slow

smoothing method applied to the domain from these locations. This created an unstructured tetrahedral grid that had the highest mesh refinement near the actual diffuser surfaces, which slowly became coarser farther away from these surfaces. A sample geometry outline of the flow configuration is shown in Fig. 3. The flow domain consists of two parts; (i) the base tunnel fan-duct and diffuser from the inlet to the exit. These regions are between the outer casing and nacelle surface, the downstream diffuser section, and the upstream inlet duct section; (ii) the downstream open rectangular wake region as shown in Fig. 3. A close up view of the sample base configuration surface mesh is shown in Fig. 4. The origin of the domain (0, 0, 0) is taken as the center of the diffuser exit section, where the flow exits to the wake in the open region (see Fig. 3 bottom). The three-dimensional domain required a large number of cells of the order of a few million to fill.

#### B. Boundary Conditions

For all computations, the no-slip condition was imposed on all solid walls or surfaces including the nacelle surface, tunnel casing wall, on the strut rod surfaces, etc. Constant pressure outlet condition was imposed on all open boundaries of the downstream rectangular wake region where the values of the velocity components are extrapolated from inside. At the diffuser casing inlet, a fully developed mean axial velocity component as obtained from Eq. (1) with average velocity compatible to the Reynolds number is used.

#### C. Grid Independence Study

In order to obtain mesh independent results, systematic mesh independence study was conducted. Starting with a basic coarse mesh with few hundred thousand cells for the baseline diffuser geometry (8BF), the mesh was successively refined. The computed velocity magnitude profiles; along the x and y directions on a vertical xy plane (3.175 mm from the end of the protruding drive shaft end;  $z = 62.552$  mm from the diffuser outlet); as well as the total pressure profiles at the diffuser entry plane (vertical xy plane at the diffuser entry;  $z = -25.716$  mm) along the diametrical y direction; were compared. The mesh was considered optimally refined when the plots of the velocity magnitude profiles and the total pressure distribution profile did not change appreciably between successive mesh refinements. For the baseline diffuser geometry (8BF), the total number of cells considered was 0.665, 1.072, and 1.477 million for each successive refinement cases. Fig. 5 shows the results of grid independence studies. It is seen that mesh independence occurs for mesh resolution beyond 1.072 million. Hence, the next higher mesh resolution (1.477 million cells) was taken for further computation for the 8BF case. Similar mesh resolutions (around 1.5 million cells) for other diffuser geometries were used in the computation. One exception to this was the diffuser geometry that made use of conical sections to split the flow at the exit of the diffuser (35FC case) where much higher mesh resolution (5.5 million cells) was needed.

### III. COMPUTATIONAL RESULTS

Numerical simulations of the diffuser flow for the four aforementioned small-scale diffuser geometries (8BT, 35BT, 35F, and 35FC) were performed using the ANSYS FLUENT code. The computational results are validated against the experimental data for all cases. The experimental data provided the velocity magnitude distributions on a measurement plane normal to the axis at immediately downstream of the nacelle drive shaft ( $z = -62.552$  mm). The predicted velocity magnitude profiles along the horizontal and vertical diametral  $x$  and  $y$  axes on the measurement  $xy$  plane are compared with the corresponding measured velocity magnitude profiles for the various diffuser geometries in Figs. 6, 7, and 8. It is seen from these comparison plots that the velocity magnitude profile trends are reasonably well captured by the computations even though there are under/over-

predictions of various magnitudes. These discrepancies can be attributed to the experimental uncertainties and computational errors. The flow domain inside the diffuser geometry is very complex due to the nacelles and supporting struts causing flow obstructions of various scales. The worst case comparison is seen to be that for the 35FC case in Figs. 6 and 7. This is because of the addition of the complicated conical section with the separating struts in between the three different cones at the diffuser end (see Fig. 1d). Nevertheless, it can be concluded that the computation provides reasonably well and reliable results, at least qualitatively. Furthermore, since qualitative comparison of the efficiencies among the different diffuser models is the goal here, quantitative accuracy is not primary concern.

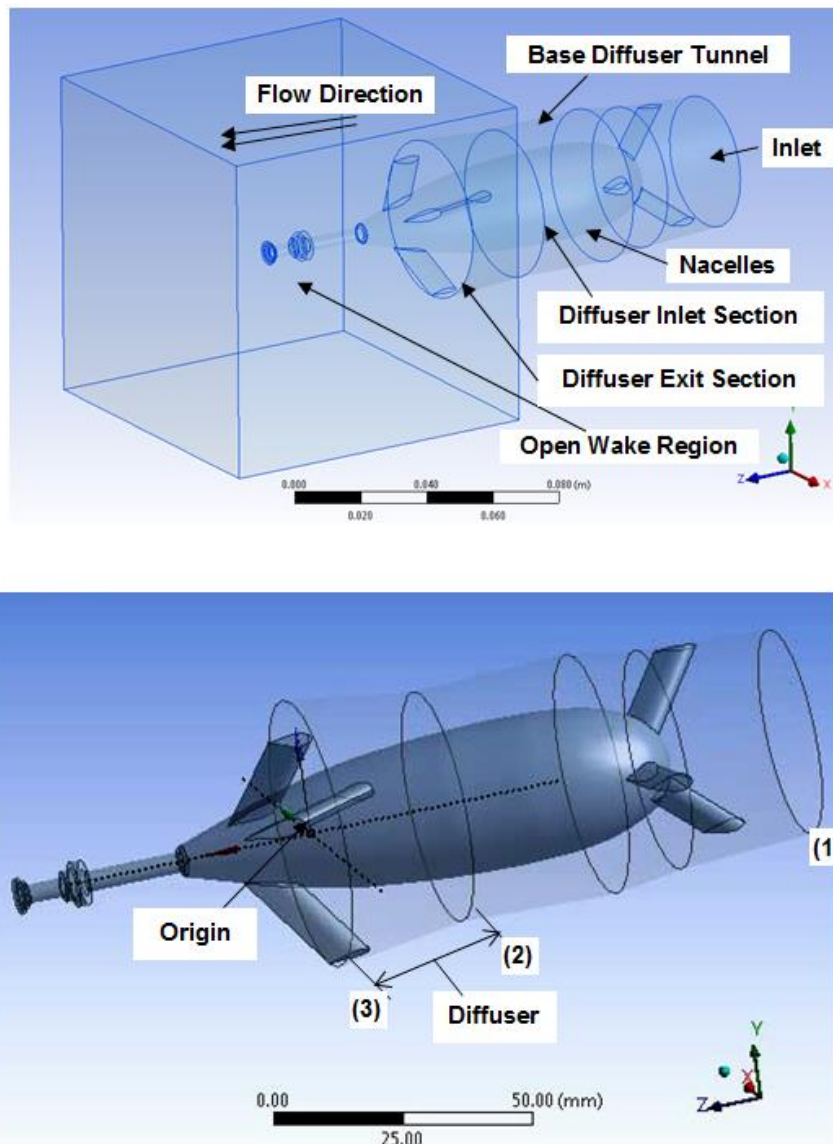
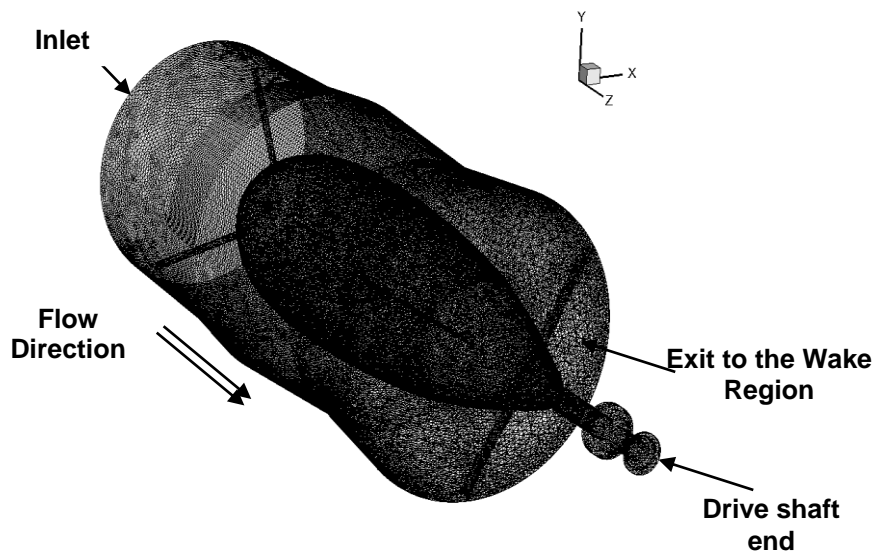
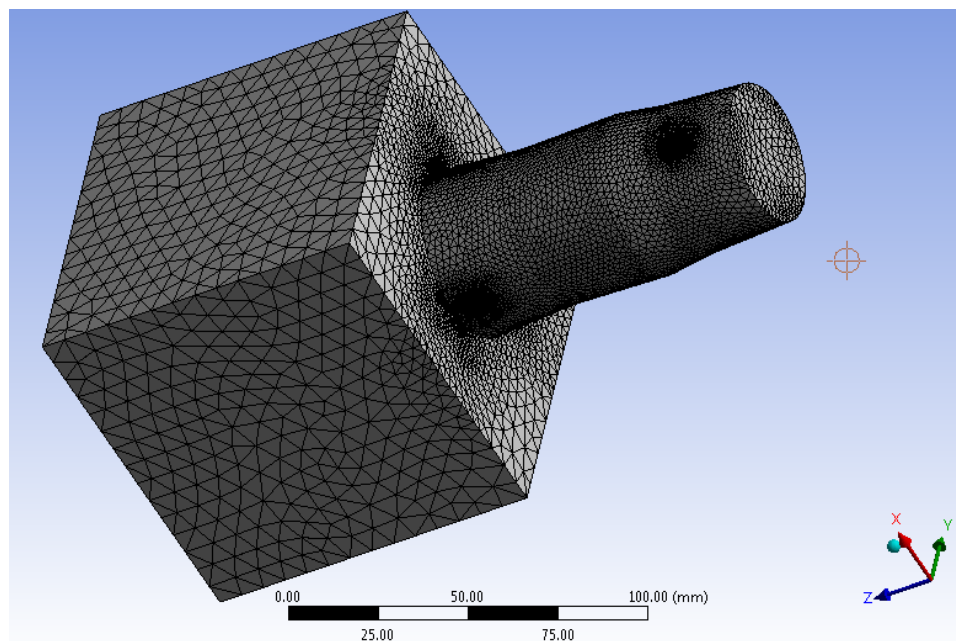


Fig. 3. Top: Outline of the flow geometry. Bottom: Close up around the nacelles and the tunnel. Colored figure available in the online version.



1.



2.

Fig. 4. Surface mesh structure; top: close up to diffuser section with the nacelles inside, bottom: whole domain.

Some further analysis and presentations of the computational results for comprehending the internal flow process are given next. First, the velocity magnitude distribution (flooded contours) on longitudinal vertical ( $yz$ ) and horizontal ( $xz$ ) planes for different diffuser geometries are presented in Fig. 9. The flow direction in this and subsequent contour plots are from left to right. The fully developed turbulent flow at the diffuser casing inlet flows toward the nacelle, creates a stagnation point at its leading nose and flows over the nacelle surface. The flow then accelerates through the annular space between the nacelle and

casing surfaces where the velocity increases to a maximum of about 90 m/s and then decelerates while passing through the diverging annular space between the rear part of the nacelle and diffuser section. The flow then leaves the diffuser section and discharges into the open region as a strong wake flow with a velocity of about 40 to 60 m/s. The development of the thin cross-stream shear layer between the wake and the surrounding stagnant air is also noticeable in these plots. This flow trend is almost similar for all diffuser configurations except for the 35FC case where the wake flow is skewed and strong turbulence is noticed

in the outer shear layer boundary. This is due to the presence of the obstructing internal conical structures and the separating struts in between the cones at the end of the diffuser section and upstream of the exit section.

One of the quantities of interest in a diffuser design is the total pressure recovery at the diffuser exit. To comprehend and compare the nature of the total pressure at the diffuser exit section ( $z = 0$ ), the contours of the same is shown in Fig. 10. The average total pressure at the inlet ( $z = -97.331$  mm, section (1) in Fig. 5 bottom) and diffuser exit section ( $z = 0$ , section (3) in Fig. 5 bottom) for the corresponding cases are given in Table 1 where the average total pressure drop are also provided. The largest total pressure drop is found to be 743.1 Pa for the 8BT case, which is the existing SARL diffuser with  $8^\circ$  half apex angle. Diffuser designs with  $3.5^\circ$  half apex angles have significantly lesser total pressure drops of 353.6 Pa, 266.9 Pa, and 255.1 Pa for the 35BT, 35F, and 35FC cases, respectively. Considering the total pressure drop as the measure of diffuser efficiency, the 35FC design happens to be the most efficient (total pressure drop 65% less than the baseline 8BT) case based on the simulations/computations performed here.

#### IV CONCLUSIONS

Computational analysis of the diffuser flow, conducted on 1:60 scale models of the diffuser section of the Air Force, Subsonic Aerodynamic Research Laboratory (SARL) wind tunnel, is conducted. The flow fields in small scale models of four diffuser geometries, identified in a previous numerical research with full scale models of these diffusers, are computed. In order to assess the validity of the numerical model and the associated numerical methods, experiments are also conducted to measure the velocity distribution in the diffuser wake for the 3D printed small scale models of the same four diffuser geometries. Comparison of the predicted and experimental velocity distributions shows reasonable agreement establishing the validity

of the computational results directly for the small scale models and indirectly for the full scale models [13].

The performance of the four diffuser design models is evaluated based on the total pressure recovery between the inlet and the diffuser exit sections. The aim is to identify the diffuser geometry generating minimum total pressure loss/drop. Results indicate that the 35FC diffuser geometry offered the greatest reduction in pressure losses. This conforms to the findings of the previous computations [13] on full scale models of the same four diffuser geometries where the 35FC diffuser design produced lowest total pressure drop.

#### NOMENCLATURE

$d$	Inlet section diameter
$g$	Gravitational acceleration
$K$	Local total pressure loss coefficient
$K_0$	Section total pressure loss coefficient
$L$	Diffuser length
$P$	Average static pressure
$P_0$	Total pressure
$\Delta P_0$	Change in total pressure across a given location
$q$	Average dynamic pressure, $P + \rho V^2/2$
$R$	Radius of the diffuser
$Re$	Reynolds number, $Re = \rho V D/\mu$
$T$	Temperature
$V$	Velocity magnitude
$V_c$	Centerline velocity at the inlet section
$x, y, z$	Coordinated directions
$\theta$	Diffuser half apex angle
$\mu$	Dynamic viscosity of fluid
$\rho$	Density of fluid

#### DECLARATION

Cleared for public Release, Unlimited Distribution, 88ABW-2013-0955, Wright Patterson Air Force Base.

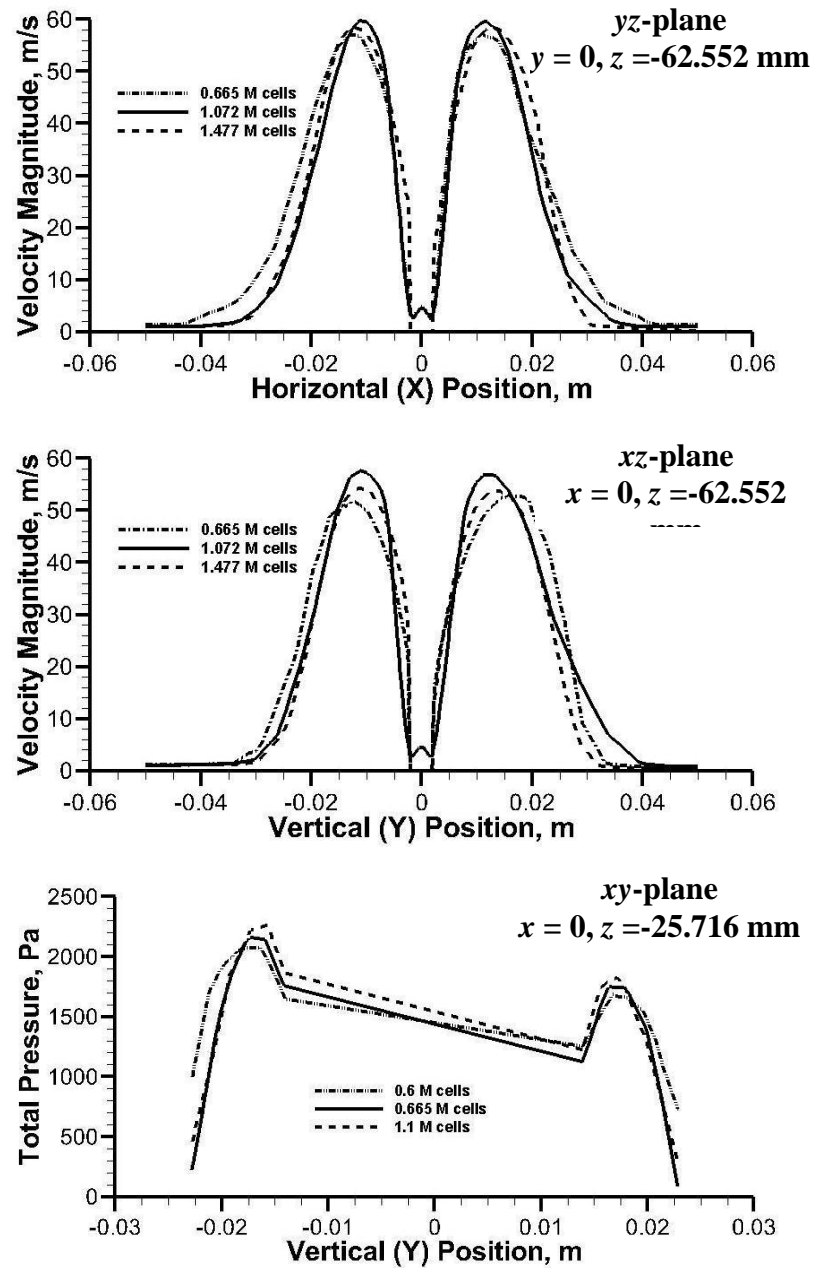


Fig. 5. Mesh refinement study.

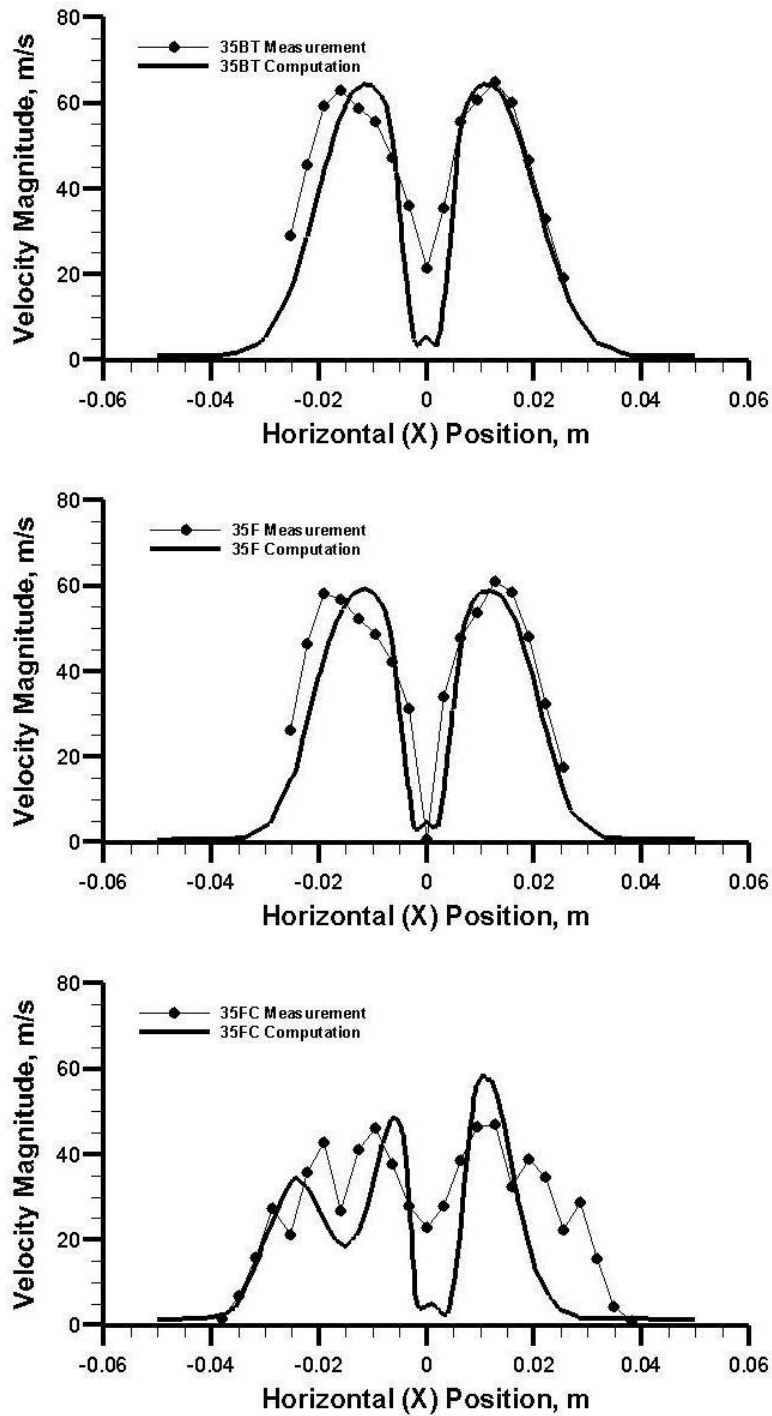


Fig. 6. Predicted velocity magnitude profiles along the horizontal diametral  $x$  axis on the measurement  $xy$  plane; compared with the corresponding measured velocity magnitude profile;  $3.5^\circ$  half apex angle diffuser cases.

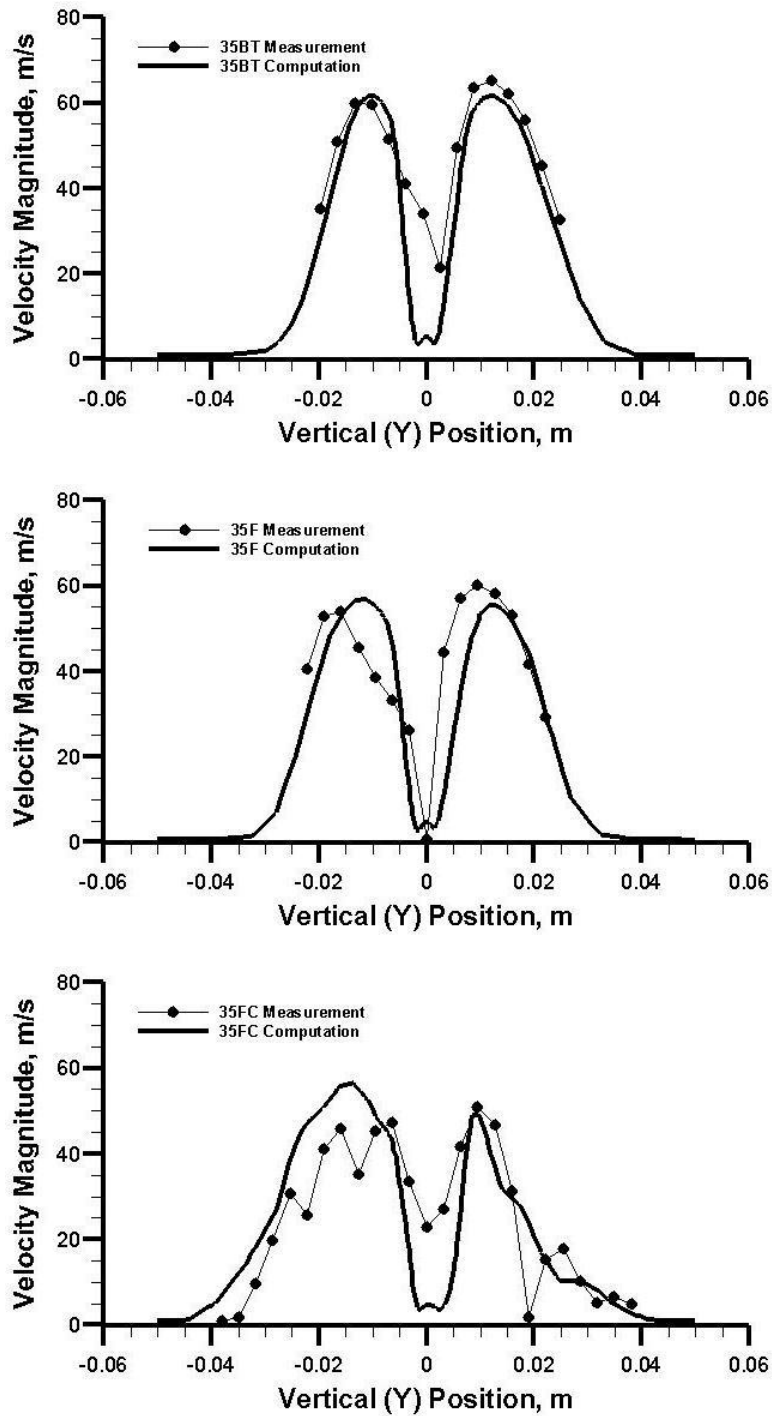


Fig. 7. Predicted velocity magnitude profiles along the vertical diametral y axis on the measurement xy plane; compared with the corresponding measured velocity magnitude profile; 3.5° half apex angle diffuser cases.

Table 1. Average total pressure at the inlet and diffuser exit section and corresponding total pressure drop.

Case	Inlet Average Total Pressure (Pa)	Diffuser Exit Average Total Pressure (Pa)	Total Pressure Drop (Pa)
8BT	1786.8	1043.7	743.1
35BT	1934.0	1580.4	353.6
35F	1636.8	1369.9	266.9
35FC	1699.3	1444.2	255.1

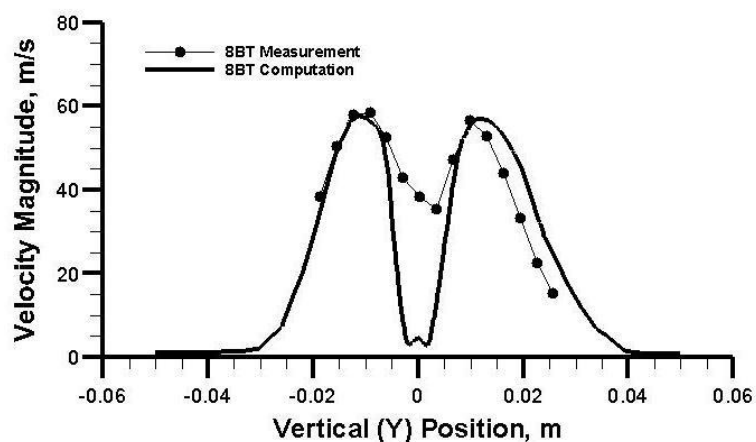
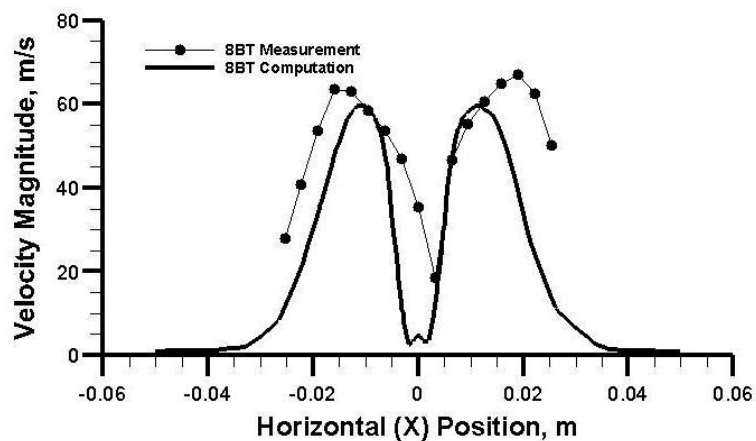


Fig. 8. Predicted velocity magnitude profiles along the horizontal and vertical diametral x and y axes on the measurement xy plane; compared with the corresponding measured velocity magnitude profile; 8° half angle diffuser case.

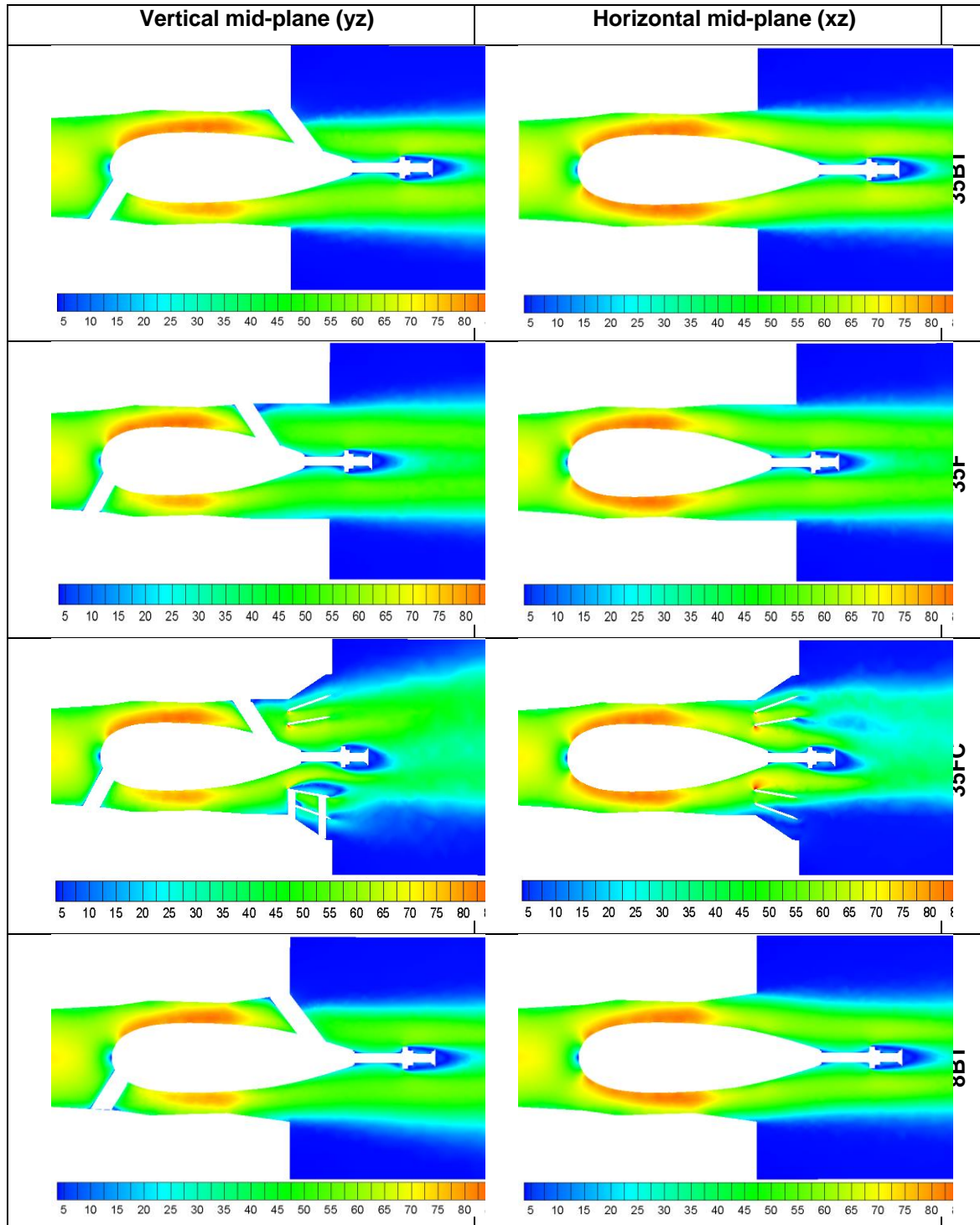


Fig. 9. Velocity magnitude (m/s) contours on the vertical mid yz-plane and on the horizontal mid xz-plane for various diffuser configurations. Flow direction from left to right. Color image available in the online version.

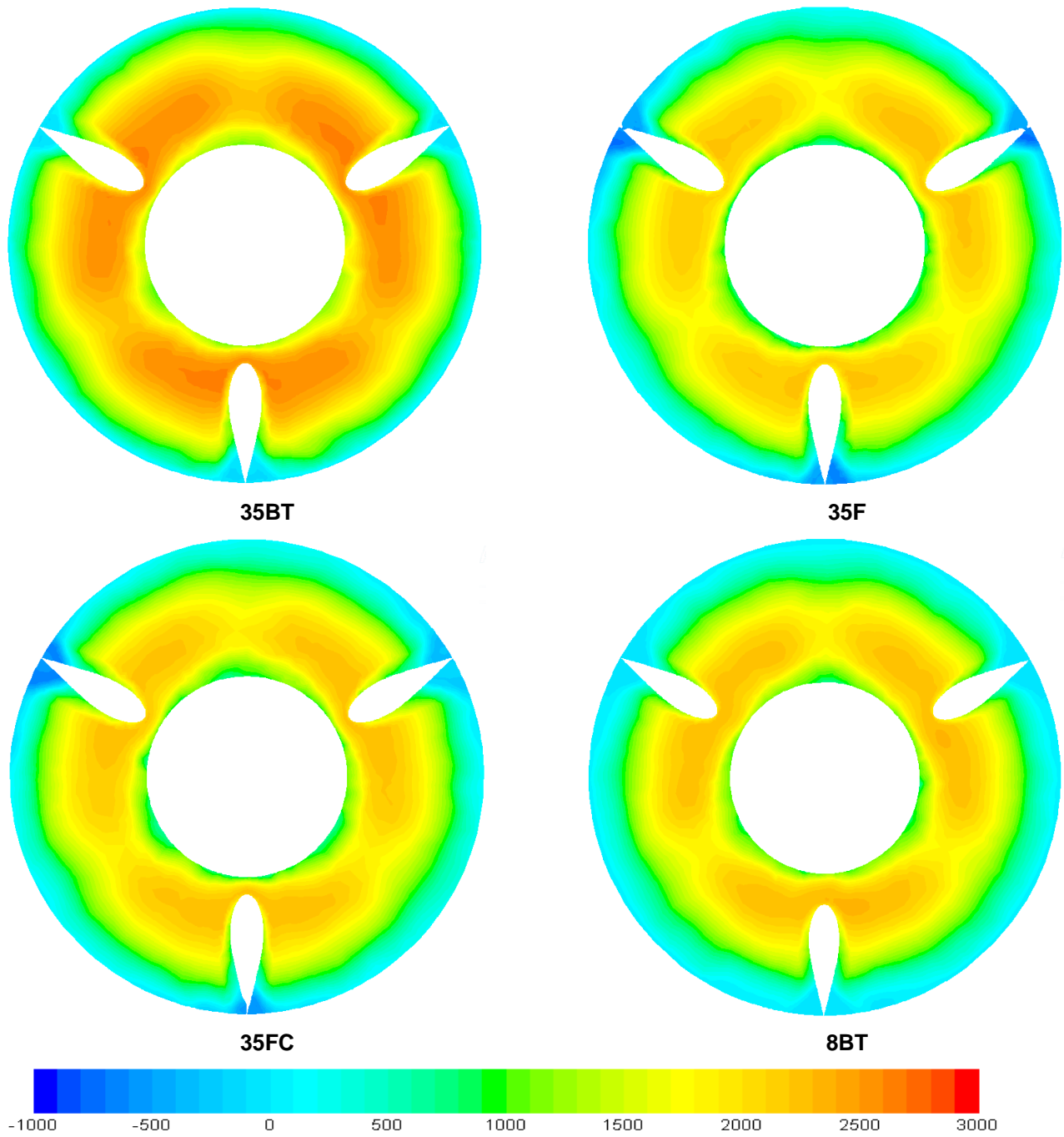


Fig. 10. Total pressure (Pa) contours on the diffuser exit  $xy$ -plane for various diffuser configurations. Color image available in the online version.

## REFERENCES

- [1] J.A. Schetz, A.E. Fuhs, Fundamentals of Fluid Mechanics, John Wiley & Sons, New York, 1999.
- [2] F.M. White, Fluid Mechanics, McGraw-Hill, New York, NY, 2003.
- [3] W.T. Eckert, K.W. Mort, J. Jope, Aerodynamic design guidelines and computer program for estimation of subsonic wind tunnel performance, NASA-TN-D-8243, A-5944 (1976).
- [4] R. Mehta, The aerodynamic design of blower tunnels with wide-angle diffusers, Prog. Aerospace Sci. 18 (1979) 59-120.
- [5] H. Li, Fluid flow analysis of a single-stage centrifugal fan with a ported diffuser, Engineering Applications of Computational Fluid Mechanics. 3 (2009) 147-163.
- [6] X. Liu, Q. Dang, G. Xi, Performance improvement of centrifugal fan by using CFD, Engineering Applications of Computational Fluid Mechanics. 2 (2008) 130-140.
- [7] S. Farokhi, Aircraft Propulsion, John Wiley & Sons, New York, NY, 2014.
- [8] V. Singhal, S.V. Garimella, J.Y. Murthy, Low Reynolds number flow through nozzle-diffuser elements in valveless micropumps, Sensors and Actuators A: Physical. 113 (2004) 226-235.
- [9] S. Singh, V. Seshadri, S. Chandel, M. Gaikwad, Analysis of the improvement in performance characteristics of S-shaped rectangular diffuser by momentum injection using computational fluid dynamics, Engineering Applications of Computational Fluid Mechanics. 3 (2009) 109-122.
- [10] S. Ghosh, D. Pratihar, B. Maiti, P. Das, Optimum design of a two step planar diffuser: a hybrid approach, Engineering Applications of Computational Fluid Mechanics. 4 (2010) 415-424.
- [11] A. McDonald, R. Fox, An experimental investigation of incompressible flow in conical diffusers, Int. J. Mech. Sci. 8 (1966) 125IN5131-130IN6139.
- [12] S. Ubertini, U. Desideri, Experimental performance analysis of an annular diffuser with and without struts, Exp. Therm. Fluid Sci. 22 (2000) 183-195.
- [13] C.D. King, S.M. Ölçmen, M.A. Sharif, T. Presdorf, Computational Analysis of Diffuser Performance for Subsonic Aerodynamic Research Laboratory Wind Tunnel, Engineering Applications of Computational Fluid Mechanics. 7 (2013) 419-432 [14] T. Presdorf, Subsonic Aerodynamic Research Laboratory, Wright-Patterson Air Force Base, WL-TR-3053. Wright-Patterson Air Force Base, WL-TR-3053 (1992).
- [15] C.P. Britcher, Analysis of the AFRL SARL Facility Drive System, Old Dominion University, Department of Mechanical and Aerospace Engineering, Norfolk, VA. (2011).
- [16] COSMOS, SOLIDWORKS Flow Simulation, (2008).
- [17] G. Sovran, E.D. Klomp, Experimentally determined optimum geometries for rectilinear diffusers with rectangular, conical or annular cross-section, FLUID MECHANICS OF INTERNAL FLOW, PROCEEDINGS OF A SUMPOSIUM, WARREN, MICH. General Motors GMR-511 (1965).
- [18] A.A. Townsend, The Structure of Turbulent Shear Flow, Cambridge university press, 1980.
- [19] A.H. Lefebvre, Gas Turbine Combustion, CRC press, 1998.
- [20] S.L. Dixon, C. Hall, Fluid Mechanics and Thermodynamics of Turbomachinery, Butterworth-Heinemann, 2013.
- [21] R.S. Azad, Turbulent flow in a conical diffuser: A review, Exp. Therm. Fluid Sci. 13 (1996) 318-337.
- [22] R.W. Fox, A.T. McDonald, P.J. Pritchard, Introduction to fluid dynamics, John Wiley & Sons. (2004).
- [23] E.M. Sparrow, J.P. Abraham, W.J. Minkowycz, Flow separation in a diverging conical duct: Effect of Reynolds number and divergence angle, Int. J. Heat Mass Transfer. 52 (2009) 3079-3083.
- [24] I. Johnston, The effect of inlet conditions on the flow in annular diffusers, AD0018166 (1953).
- [25] V. Ganesan, Flow and boundary layer development in straight core annular diffusers, Int. J. Eng. Sci. 18 (1980) 287-304.
- [26] S. Shuja, M. Habib, Fluid flow and heat transfer characteristics in axisymmetric annular diffusers, Comput. Fluids. 25 (1996) 133-150.
- [27] E.M. Cherry, A.M. Padilla, C.J. Elkins, J.K. Eaton, Three-dimensional velocity measurements in annular diffuser segments including the effects of upstream strut wakes, Int J Heat Fluid Flow. 31 (2010) 569-575.
- [28] K.P. Lo, C.J. Elkins, J.K. Eaton, Separation control in a conical diffuser with an annular inlet: center body wake separation, Exp. Fluids. 53 (2012) 1317-1326.
- [29] Ansys Incorporated, Ansys Fluent Version 14, (2015).
- [30] B.R. Munson, D.F. Young, T.H. Okiishi, Fundamentals of Fluid Mechanics, John Wiley & Sons, New York, NY, 1990.
- [31] S. Kline, F. McClintock, Describing uncertainties in single-sample experiments, Mech. Eng. 75 (1953) 3-8.